Structure
Article

Cdc13 OB2 Dimerization Required for Productive Stn1 Binding and Efficient Telomere Maintenance

Mark Mason,[1,2] Jennifer J. Wanat,[3] Sandy Harper,[1] David C. Schultz,[1] David W. Speicher,[1] F. Brad Johnson,[3] and Emmanuel Skordalakes[1,2,*]
[1]The Wistar Institute, 3601 Spruce Street, Philadelphia, PA 19104, USA
[2]Department of Chemistry, University of Pennsylvania, Philadelphia, PA 19104, USA
[3]Department of Pathology and Laboratory Medicine, University of Pennsylvania, Stellar-Chance 405A, 422 Curie Boulevard, Philadelphia, PA 19104, USA
*Correspondence: skorda@wistar.org
http://dx.doi.org/10.1016/j.str.2012.10.012

SUMMARY

Cdc13 is an essential yeast protein required for telomere length regulation and genome stability. It does so via its telomere-capping properties and by regulating telomerase access to the telomeres. The crystal structure of the *Saccharomyces cerevisiae* Cdc13 domain located between the recruitment and DNA binding domains reveals an oligonucleotide-oligosaccharide binding fold (OB2) with unusually long loops extending from the core of the protein. These loops are involved in extensive interactions between two Cdc13 OB2 folds leading to stable homodimerization. Interestingly, the functionally impaired *cdc13-1* mutation inhibits OB2 dimerization. Biochemical assays indicate OB2 is not involved in telomeric DNA or Stn1 binding. However, disruption of the OB2 dimer in full-length Cdc13 affects Cdc13-Stn1 association, leading to telomere length deregulation, increased temperature sensitivity, and Stn1 binding defects. We therefore propose that dimerization of the OB2 domain of Cdc13 is required for proper Cdc13, Stn1, Ten1 (CST) assembly and productive telomere capping.

INTRODUCTION

Telomeres are nucleoprotein structures consisting of telomeric DNA (Blackburn and Gall, 1978) and protein assemblies, such as the CST (Cdc13, Stn1, Ten1) complex, that localize to the ends of chromosomes (Baumann et al., 2002; Miyake et al., 2009; Nakaoka et al., 2012; Song et al., 2008; Surovtseva et al., 2009; Wellinger, 2009). Telomeres form protective caps that prevent chromosome termini from behaving as generic DNA double-stranded breaks (Lin and Zakian, 1996; Miyake et al., 2009; Wang et al., 2007), which could otherwise lead to genomic instability and cellular senescence (Garvik et al., 1995; Grandin et al., 2001). The yeast CST trimeric complex, a RPA-like complex (Gao et al., 2007; Gelinas et al., 2009; Sun et al., 2009) consisting of Cdc13, Stn1, and Ten1, facilitates chromosome end capping and promotes telomerase and polα recruitment to the telomeres (Grandin et al., 1997, 2001; Pennock et al., 2001; Qi and Zakian, 2000; Wellinger, 2009; Xu et al., 2009). CST capping requires localization of Cdc13 to the telomeric ends, accomplished by the tight association of the DNA binding domain (DBD [OB3]) to short stretches ($\geq$11 bases) of single-stranded, telomeric DNA (sstDNA) (Mitton-Fry et al., 2002, 2004; Nugent et al., 1996) and in some cases in proximity of the double/single-stranded DNA junction at telomeres, where there may be competition of binding with Rap1 (Gustafsson et al., 2011).

Cdc13, like a number of single-stranded telomere binding proteins, including the ciliate *Oxytricha nova* telomere end binding protein (OnTEBP) (Horvath et al., 1998) as well as the human and *Schizosaccharomyces pombe* Pot1 (Lei et al., 2003, 2004; Nandakumar et al., 2010), consists of several OB folds. These folds potentially arise from evolutionary gene duplication and are involved in multiple functions, including nucleic acid and protein binding and Cdc13 dimerization (Mitchell et al., 2010; Mitton-Fry et al., 2002, 2004; Sun et al., 2011; Yu et al., 2012). Yeast full-length Cdc13 dimerization is mediated at least by its N-terminal domain (OB1), and in the case of the yeast *Candida galbrata* and *Candida tropicalis* dimerization is mediated by the C-terminal domain (CTD) (OB4) of the protein (Mitchell et al., 2010; Sun et al., 2011; Yu et al., 2012). OB1 has weak affinity for long sstDNA and is involved in Cdc13 dimerization and recruitment of Polα-primase to the telomeres for C-strand synthesis (Mitchell et al., 2010; Sun et al., 2011). The ability of OB1 to bind long telomeric overhangs depends directly on its dimerization properties, suggesting that this domain is highly specialized to function during late S to G2 phase when the telomeric overhang is long, thus regulating access of telomerase to the telomeres. Moreover, Cdc13 (OB1) dimerization may also be essential for efficient telomerase recruitment to the telomeres, as yeast telomerase acts as a dimer (Prescott and Blackburn, 1997). Disruption of the OB1 dimerization leads to shorter telomeres, suggesting that Cdc13 is defective in telomerase recruitment to the telomeres. In contrast to OB1, disruption of the *Candida tropicalis* Cdc13, OB4 dimer affects its ability to bind long telomeric DNA (Yu et al., 2012).

The ability of Cdc13 to perform two opposing functions, in particular to cap the ends of chromosomes by its association

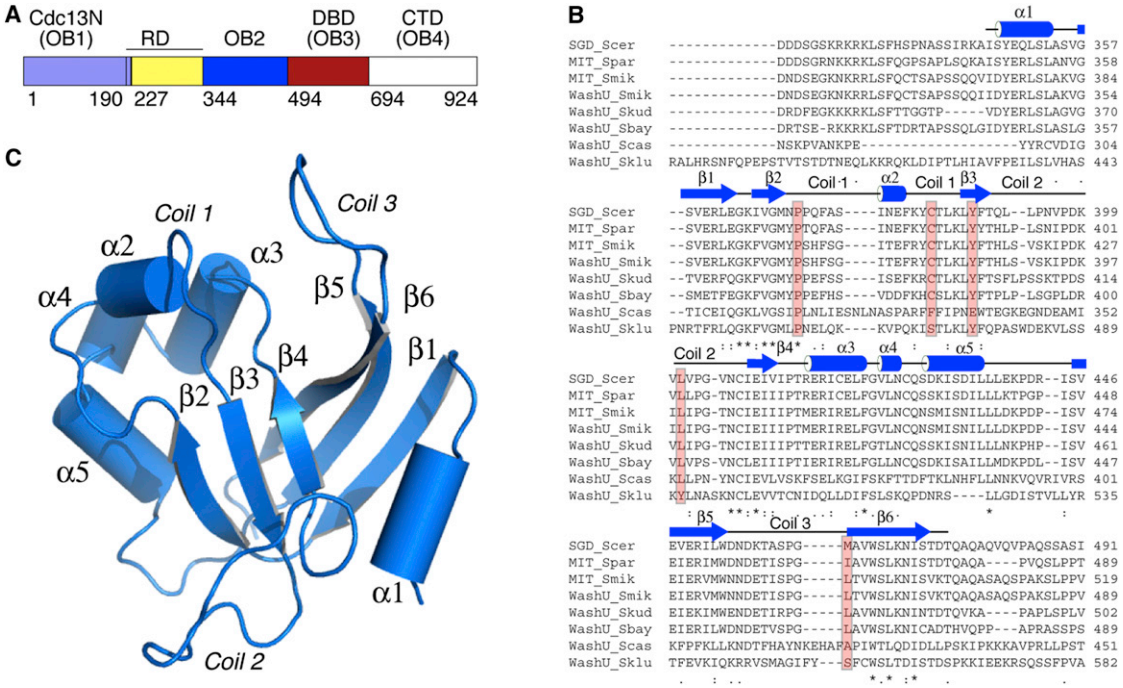

Figure 1. Primary and Tertiary Structure of the Cdc13, OB2 Monomer

(A) *S. cerevisiae* Cdc13 domain organization. The Cdc13N (OB1), RD, OB2, DBD (OB3), and CTD (OB4) are shown in light blue, yellow, blue, red, and white, respectively.

(B) Sequence alignment of the Cdc13(OB2), showing secondary structural elements and residues mutated in this study, are in red.

(C) Crystal structure of the OB2 with structural elements labeled.

with the Stn1/Ten1 complex and also to facilitate telomerase recruitment to the telomeres via its interaction with the telomerase RNA associated protein, Est1 is mediated by its recruitment domain (RD), located just downstream of the OB1 (Chandra et al., 2001; DeZwaan et al., 2009; Li et al., 2009; Pennock et al., 2001; Tseng et al., 2006). Interestingly, both Stn1 and Est1 bind to the RD domain, which has led to the proposal that Stn1 and Est1 have partially overlapping binding sites (Chandra et al., 2001; Nugent et al., 1996; Wang et al., 2000). These apparently opposing activities of Cdc13 are modulated by Hsp82 (DeZwaan et al., 2009) and Cdck1-dependent phosphorylation of the RD domain of Cdc13 (Li et al., 2009), which facilitates the switch between the DNA-bound and accessible state of the telomeric overhang for telomere elongation by telomerase. However, additional evidence suggests that Stn1 also interacts at the C terminus of Cdc13, several hundred amino acids away from the RD domain (DeZwaan et al., 2009; Hang et al., 2011).

Directly downstream of the RD and upstream of the DBD (OB3) lies a structurally uncharacterized domain. The functionally impaired Cdc13-1 protein contains the P371S mutation within this domain. Also known as a temperature-sensitive mutation, it has been shown to induce telomere uncapping (an effect enhanced at nonpermissive temperatures) as shown by elongated telomeres, exonuclease-mediated C-strand degradation (Maringele and Lydall, 2002; Paschini et al., 2012; Zubko et al., 2004), and Rad9-dependent cell-cycle arrest induced by the resulting single-stranded G-strand (Garvik et al., 1995). To further elucidate the role of the domain located between the RD and the DBD (OB3) and the mechanism of *Cdc13-1*-induced telomere uncapping, we solved the crystal structure of this region to 2.3 Å resolution. The structure revealed an OB fold involved in self-dimerization, which we will refer to as OB2 as it is the second OB-fold counting from the N terminus of Cdc13. Contacts between the two OB2 monomers are remarkably extensive, spanning 3,280 Å^2, indicating this may comprise the core dimerization domain of Cdc13. The OB fold indentation, which usually participates in nucleic acid or peptide binding is buried at the core of the OB2 dimer and is therefore not accessible for such interactions. Indeed, biochemical studies show that this domain does not associate with sstDNA or Stn1. The data presented here and the location of the OB2 with respect to the RD and DBD (OB3) domains suggest that OB2 dimerization is essential for proper CST assembly and productive telomere capping.

RESULTS

Structure of the Cdc13 OB2 Domain

To elucidate the role of the *Saccharomyces cerevisiae* Cdc13 OB2, we solved the structure of the Cdc13 domain comprising residues 344 to 494, identified by limited proteolysis (Figures 1A and 1B). There was clear density for amino acids 346 to 474. The structure revealed a core of six antiparallel β strands arranged into a β-barrel, flanked by five α helices (Figure 1C), a fold that belongs to the family of oligonucleotide/oligosaccharide binding (OB-fold) proteins. A striking feature of this domain

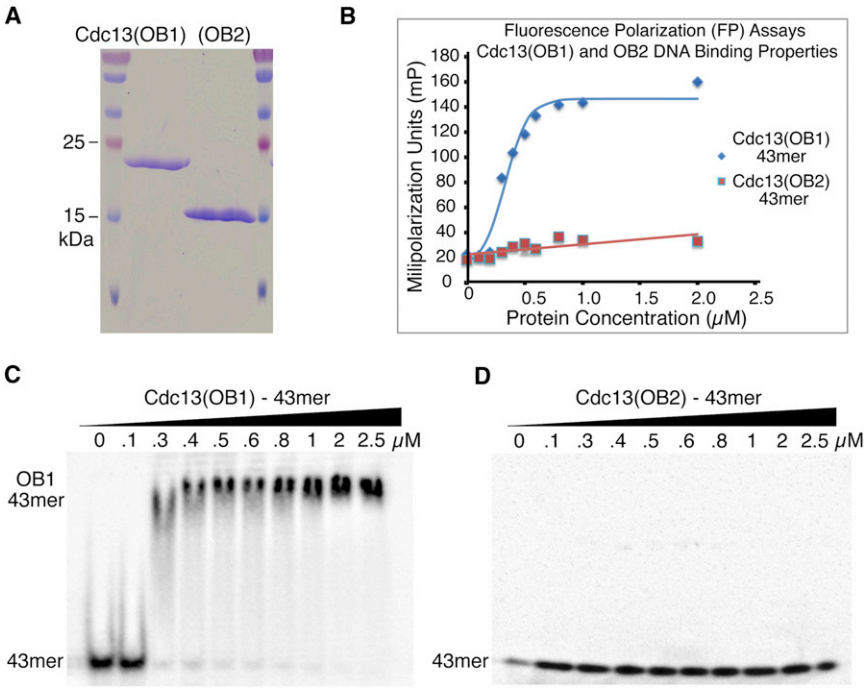

Figure 2. DNA Binding Properties of the Cdc13, OB1, and OB2 Proteins

(A) SDS-PAGE gel of the Cdc13N (OB1) and OB2 proteins.

(B) Fluorescence polarization assays of Cdc13N (OB1 - blue line) and OB2 (red line) with the single-stranded, yeast, telomeric DNA 43-mer (Table S1). The sigmoidal shape of the plot of the Cdc13N(OB1) - 43-mer data, suggests cooperative binding.

(C and D) Electrophoretic mobility shift assays (EMSA) of Cdc13N (OB1) and OB2 with the 43-mer, respectively.

are three extended coils (coil 1, 2, and 3; Figure 1C) that protrude from the core of the β-barrel, and which, as we will discuss later, are essential for Cdc13 function. A survey in the Protein Data Bank (PDB) database using the Dali server did not identify any close structural homologs of Cdc13 OB2. Cdc13 OB2 is most similar to the *C. glabrata* Cdc13 OB4 with a Z score of 9.1 and a root-mean-square deviation (rmsd) of 2.8 Å. The structural and functional differences between the four Cdc13 OB folds lie with the diversity and organization of the loops and helices located on the surface of these domains. However, the core (β-barrel) structural organization among the Cdc13 OB1, OB2, DBD (OB3), and OB4 domains is relatively conserved with an overall rmsd of ~2.6 Å.

Cdc13 OB2 Does Not Bind Telomeric DNA or Stn1

Cdc13 binds sstDNA using at least two distinct OB folds. These include the DBD (OB3), which binds sstDNA consisting of a minimum of 11 bases with high affinity (Mitton-Fry et al., 2002), and the Cdc13N (OB1), which binds long sstDNA (>35 bases) (Figures 2A–2C) in a co-operative manner with a K_d of approximately 500 nM (Figures 2B and 2C). In contrast to the DBD (OB3) and OB1, OB2 does not bind even long telomeric DNA at an appreciable level (Figures 2A, 2B, and 2D) independently of the full-length protein. We then asked if OB2 is involved in contacts with Cdc13's interacting partner Stn1. To address this question we performed isothermal titration calorimetry (ITC) assays using OB2 at a constant concentration and titrated in the C-terminal domain of Stn1, consisting of residues 311–494 (Stn1C) and comprising the Cdc13-interacting portion of the protein (Puglisi et al., 2008). The N-terminal portion of Stn1 is involved in Ten1 binding and is dispensable for Cdc13 binding (Grandin et al., 2001; Martín et al., 2007; Xu et al., 2009). The data clearly indicates that OB2 does not bind Stn1 (Figure S1A available online).

Cdc13 OB2 Facilitates Cdc13 Dimerization

The Cdc13 OB2 structure revealed two monomers in the asymmetric unit held together by extensive protein-protein and solvent-mediated interactions, spanning 3,280 Å^2 of the surface area of each monomer (Figure 3A). Interestingly, the indentation on the surface of the OB fold, usually involved in substrate binding, is buried within the dimerization interface of the two subunits and is not solvent accessible for nucleic acid or peptide binding (Figure 4A). Several lines of evidence support the conclusion that OB2 dimerizes, including specific crosslinking experiments on the recombinant OB2 domain at 0.5–1 mg/ml using 0.3% formaldehyde solution, which has one of the shortest spans (2–3 Å) of any crosslinking reagent and therefore is an ideal tool for detecting specific protein-protein interactions (Nadeau and Carlson, 2007a, 2007b, 2007c). The crosslinked samples were run on a denaturing 15% SDS-PAGE gel, and the band intensities were analyzed using ImageJ (Abramoff et al., 2004). The results clearly show a shift of the OB2 monomeric band (17 kDa) to a band corresponding to 34 kDa, which corresponds to a dimeric OB2 (Figures 3B and 3C). This is further illustrated by the fact that the negative control Stn1C, which is monomeric in solution, does not show crosslinking at the same protein concentration (Figures 3B and 3C). Cdc13 OB2 dimerization is also supported in solution by size-exclusion chromatography. To further analyze the oligomeric state of the OB2 protein, we ran the protein on a Superdex S200 column of 24 ml bed volume (GE Healthcare, Waukesha, WI, USA) and at varying salt concentrations (100, 250, or 500 mM KCl). Figure 3D shows the OB2 protein elutes at a volume of 15.9 ml corresponding to an ~31 kDa mass, the size of a dimeric Cdc13 OB2 (molecular standards for this column are shown in Figure S2A).

We also tested the oligomeric state of the protein using dynamic light scattering (DynaPro Titan - Wyatt Technology Co., Goleta, CA, USA). Dynamic light scattering was carried out at three different salt (100, 250, and 500 mM KCl), and glycerol (0%, 2.5%, and 5%) concentrations. The above conditions were tested at two different temperatures (4°C and 18°C). All samples showed a single peak (100% mass) at ~2.78 nM, which corresponds to a 38 kDa particle, the size of a dimeric

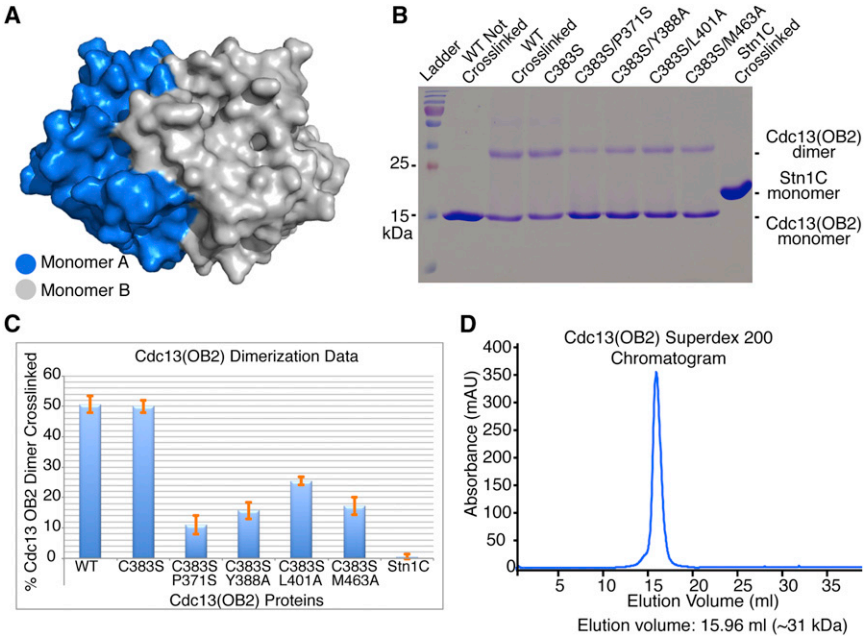

Figure 3. Cdc13 OB2 Dimerization Evidence

(A) Surface representation of the OB2 dimer showing extensive interactions between monomer A (blue) and monomer B (gray).

(B) SDS-PAGE gel of the formaldehyde crosslinked WT and mutant Cdc13, OB2 proteins.

(C) Crosslinking efficiencies of WT and mutant OB2 as analyzed by ImageJ; the orange bars indicate error associated with the measurements. Each experiment was carried out in triplicate, and the error bar represents the standard deviation of the average difference between the three measurements.

(D) Size-exclusion chromatogram (Superdex S200 – GE Healthcare) of the WT OB2 protein shows a stable dimer (see also Figure S2A for standards).

OB2 (Figure S2B). Moreover a second crystal form ($P432_12$) grown under different crystallization conditions showed precisely the same dimer organization (Figure S2C) as the orthorhombic crystals. The ability of OB2 to dimerize is most likely enhanced in the context of the full-length protein, where the two OB2 domains are brought in proximity of each other because of Cdc13 dimerization also mediated by the N- and C-terminal portions of the protein.

It is worth noting that the dimerization surface area of OB2 is more than three times that of the Cdc13 OB1 dimer and involves a host of interactions between conserved residues. A large number of the dimerization contacts involve residues that form part of the extended loops (coils 1, 2, and 3; Figures 1C and 4B) and helices (α2) that protrude from the core of the β-barrel. Additional dimerization contacts are mediated by residues located on the surface of the β-barrel. For example, the residue P371, which is mutated to a serine in the *Cdc13-1* temperature-sensitive mutant, plays a critical role in OB2 dimerization. The residue P371 facilitates the termination of the β2 strand and the initiation of a long coil (coil 1) that extends like a tentacle from the core of the β-barrel (Figure 4B). Coil 1 is involved in extensive contacts with helices α3, α4, and α5 of the same monomer (Figures 5A and 5B), thus contributing to the fold of the protein. In particular F374, I377, F380, and L385 of coil 1 make extensive hydrophobic interactions with I412, I418, V424, C427, and I432 that form part of helices α3, α4, and α5 (Figure 5B). Coil 1 also makes extensive solvent and protein-mediated interactions with coils 1 and 2 of the adjacent monomer, thus facilitating Cdc13 OB2 dimerization (Figure 4B). In particular, P371 and P372 sit in a shallow pocket formed by the backbone of Y382 and C383 as well as the aliphatic part of the side chains of N455 and E456 of coils 1 and 2, respectively, of the adjacent monomer (Figures 4C and 4D). In turn, the side chain of Y382 abuts the backbone of Q373 and F374 and interacts with the aliphatic part of the side chain of Q373 (Figure 4C). An interesting feature of this coil is the presence of a buried disulfide bond. This bond is formed between residues C383 on the same coil of each monomer and is most likely involved in stabilizing the core of the homodimer (Figure 4C).

The coils that connect strands β3-β4 (coil 2) and β5-β6 (coil 3) also extend from the core of the OB-fold and are involved in contacts with the adjacent monomer also contributing to the stabilization of the homodimer (Figure 4B). Of particular note are the residues L401, V402, and P403 of coil 2 and N455, E456, P461, and M463 of coil 3 as well as the side chain of Y388 that forms part of β3 (Figure 4D). L401, P403, and Y388 extend toward the surface of the adjacent monomer and make extensive hydrophobic interactions with the side chain of P461 and M463. The smaller side chain of V402 makes limited contacts with A464 of the adjacent monomer (Figure 4D). Interestingly, contacts between L401 and P403 of coil 2 with V367 and Y388 of the β-barrel facilitate the organization of this structural element, which in turn plays an important role in the fold (via contacts of Y348 of helix α1 with I408 and L392 of coil 2) and dimerization of the domain (Figure 5C).

Cdc13 OB2 Dimerization-Deficient Mutations Disrupt Stn1 but Not DNA Binding of the Full-Length Protein In Vitro

To further elucidate the role of OB2 homodimerization in Cdc13 function, we tested the ability of the full-length (fl), wild-type (WT) Cdc13 proteins and the mutations that disrupt Cdc13 OB2 dimerization for Stn1 binding using isothermal titration calorimetry (ITC) and DNA binding using electrophoretic mobility shift (EMSA) and fluorescence polarization (FP) assays. The C383S mutation, which was designed to eliminate the disulfide bond between the two OB2 monomers, did not disrupt OB2 dimerization (Figures 3B and 3C). This is not surprising considering the extensive interactions between the OB2 dimer interface (3,280 $Å^2$). We therefore introduced double mutations consisting of C383S and one of the following conserved

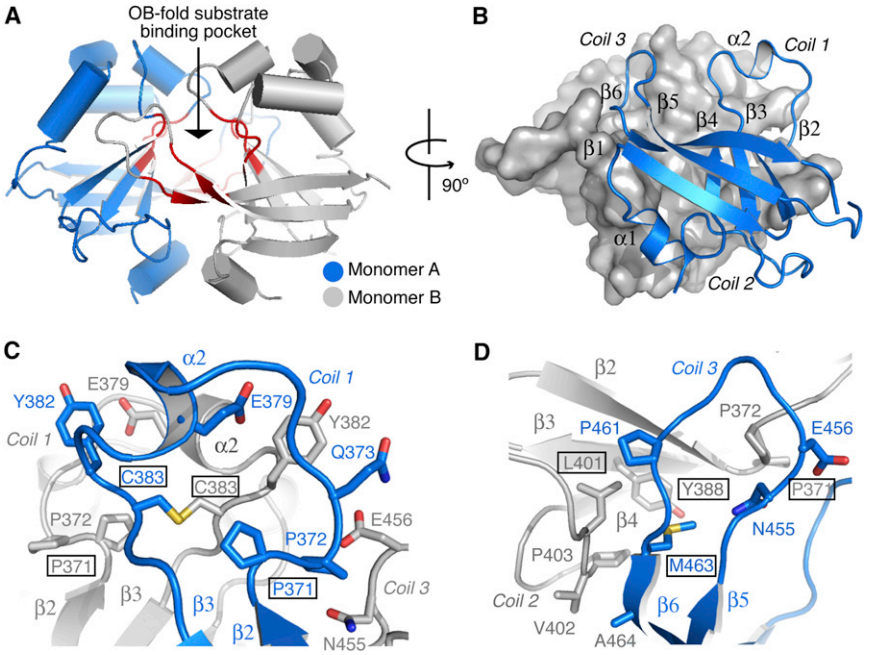

Figure 4. Dimerization Interface of the Cdc13 OB2 Domain

(A) The substrate binding pocket (red) of OB2 is buried within the dimer.

(B) Cartoon (monomer A) and surface (monomer B) representation of the OB2 dimer showing the extent of the dimerization interface and the role of the three coils in dimer formation.

(C) Cdc13 OB2 dimer contacts mediated by coil 1; residue P371 (boxed) terminates β2, forming a kink and initiating coil 1. This specific organization allows for multiple hydrophobic interactions, as well as the formation of a disulfide bond between C383 of each monomer.

(D) Cdc13 OB2 dimer contacts mediated by the conserved residues Y388, L401, and M463 (boxed) that form part of coil 3.

residues P371, Y388, L401, and M463 (which appear to disrupt OB2 dimerization in the OB2 crosslinking experiments; Figures 3B and 3C) to the flCdc13. To perform these assays, we overexpressed and purified the full-length, WT, and double-mutant Cdc13 proteins (C383S/Y388A, C383S/L401A, and C383S/M463A) as well as Stn1C to homogeneity using affinity and size-exclusion chromatography (Figures 6A and 6B; Figure S2D). It is worth noting that the full-length Cdc13 mutant proteins, designed to disrupt OB2 dimerization, remain oligomeric in solution (Figure S2D) as they are still held together by tight interactions between the OB1 and possibly OB4 homodimers. ITC studies showed that Stn1C binds to WT Cdc13 at 20°C and 30°C with a K_d of about 1.5 μM (Figures 6B, 6C, and S1B), which is well within the range of biologically relevant protein-protein interactions (Kaushansky et al., 2010; Sharma et al., 2009), whereas the flCdc13 dimerization mutants did not show detectable Stn1 binding even at 40 μM Cdc13 concentration (Figures 6B–6H). Moreover, we show that the Cdc13 construct consisting of residues 344–924 (domains OB2-DBD-OB4) has 4-fold weaker Stn1C affinity (K_d 6.4 μM; Figure S1C), than the wild-type, flCdc13. The ITC data supports contacts of Stn1 with the N-terminal portion of Cdc13, which is in agreement with earlier data (Chandra et al., 2001; Nugent et al., 1996; Wang et al., 2000).

To determine if the OB2 dimerization-deficient mutants that disrupt Stn1 binding were active, we tested their ability to bind sstDNA. To address this question, we performed EMSA and FP assays using a yeast telomeric DNA 12 bases long (the 11-mer with a T added at the 5′ end, which has been shown previously to bind flCdc13 and the DBD [OB3] proteins with high affinity; Hughes et al., 2000; Table S1) and the WT and mutant flCdc13 proteins, C383S, C383S/P371S, C383S/Y388A, C383S/L401A, and C383S/M463A, which had been purified to homogeneity (Figure S2D). The FP assays were performed using 5 nM of fluorescently labeled DNA probe and 0 to 50 nM flCdc13, whereas the EMSA were performed using 0.5 nM DNA and 0 to 100 nM protein. Both assays showed wild-type DNA binding for all four mutants (Figures 7A–7H), clearly suggesting that these proteins are active but defective in Stn1 binding (Figures 6A–6D) and efficient CST assembly.

Dimerization-Deficient Mutations Elicit Telomere Length and Growth Defects In Vivo

To further investigate the effect of the OB2 dimerization mutants in vivo, we examined one single and five double-point mutants for temperature-dependent changes in cell viability using spot assays or telomere length using Southern blots (Figure 8). Mutations were created in ARS/CEN plasmids

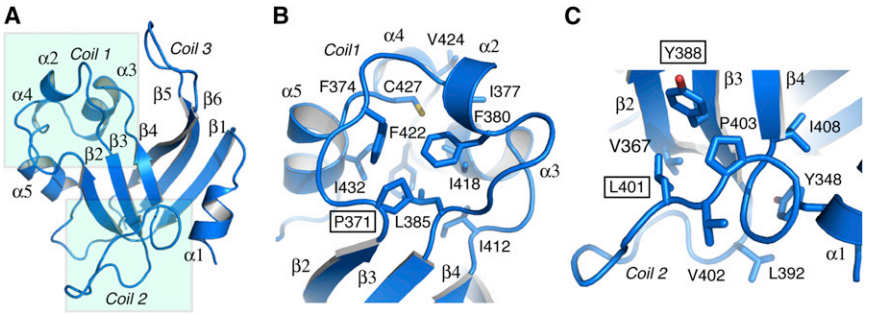

Figure 5. Role of Coils 1 and 2 in OB2 Protein Fold

(A) Structure of the OB2 monomer. Coils 1 and 2 are highlighted, and structural elements are labeled.

(B) Structural organization of coil 1 and its contacts with helices 3 and 4 of the same monomer.

(C) Structural organization of coil 2 and its contacts with helix α1 and the β-barrel.

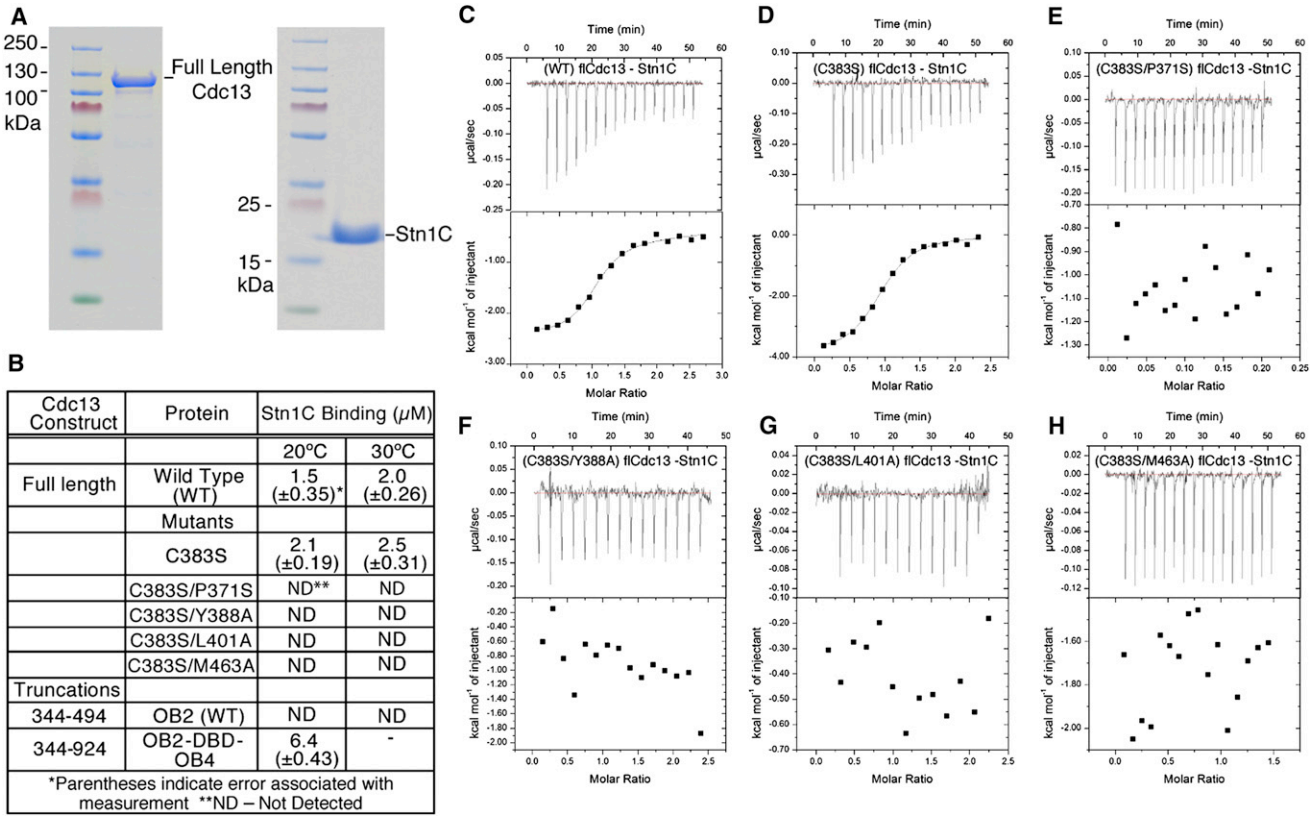

Cdc13 Construct	Protein	Stn1C Binding (µM)	
		20°C	30°C
Full length	Wild Type (WT)	1.5 (±0.35)*	2.0 (±0.26)
	Mutants		
	C383S	2.1 (±0.19)	2.5 (±0.31)
	C383S/P371S	ND**	ND
	C383S/Y388A	ND	ND
	C383S/L401A	ND	ND
	C383S/M463A	ND	ND
Truncations			
344-494	OB2 (WT)	ND	ND
344-924	OB2-DBD-OB4	6.4 (±0.43)	-

*Parentheses indicate error associated with measurement **ND – Not Detected

Figure 6. Stn1 Binding Properties of the WT and Mutant flCdc13 Proteins

(A) SDS-PAGE gel of flCdc13 and Stn1C.

(B) Table of ITC values for the full-length, WT, single-mutant, and double-mutant Cdc13 proteins obtained from the curve fit of Figures 6C–6H.

(C–H) ITC raw data of Stn1C with any of the following flCdc13 proteins at 20°C: (C) wild-type, (D) C383S, (E) C383S/P371S, (F) C383S/Y388A, (G) C383S/L401A, and (H) C383S/M463A. The temperature changes upon Stn1C injections to the cell containing the flCdc13 are shown on the top and enthalpies, with binding curve fit if applicable, are on the bottom. See also Figure S1.

expressing full-length Cdc13 under the control of its own promoter and transformed into *CDC13/cdc13Δ* diploid *S. cerevisiae*, which were then sporulated to obtain haploid *cdc13Δ* strains bearing each plasmid. The single C383S mutation (designed to disrupt disulfide bond formation) had no effect in either assay, consistent with its lack of effect on dimerization (Figures 3B and 3C). However, strains containing plasmids with C383S and one of the following: P371S, Y388A, L401A, and M463A mutations, showed temperature-dependent changes in telomere length and/or cell viability (Figures 8A and 8B), consistent with loss of Stn1 binding and telomere uncapping. At room temperature (22°C), all of the mutants were viable although longer telomeres were observed for the P371S mutant, consistent with previous studies (Grandin et al., 1997). At 30°C, the P371S mutant is inviable in agreement with published data (Nugent et al., 1996), whereas the Y388A mutant grew poorly. At this temperature, slightly longer telomeres are observed with the Y388A and M463A mutants (Figures 8A and 8B). At 37°C, Y388A is inviable, whereas L401A exhibited a mild growth defect and a slight increase in telomere length. The M463A mutation at 30°C caused slight telomere lengthening without a significant growth defect (Figure 8B). At 37°C all the mutant and WT Cdc13 proteins show significantly shorter telomeres than they do at 22°C or 30°C, consistent with previous work (Paschini et al., 2012).

DISCUSSION

Cdc13's ability to bind nucleic acid and protein substrates and carry out its function depends on several OB folds (Mitchell et al., 2010; Mitton-Fry et al., 2004; Sun et al., 2011; Yu et al., 2012) and self-dimerization, which has so far been shown to be mediated by the OB1 in *S. cerevisiae* (Mitchell et al., 2010; Sun et al., 2011) and OB4 in *C. galbrata and C. tropicalis* (Yu et al., 2012). Here, we show that OB2, a domain located between the RD and DBD (OB3) domains, is also involved in self-dimerization of *S. cerevisiae* Cdc13, a process mediated by a host of interactions that span 3,280 Å^2 of the surface of the molecule. Previously, we showed that disruption of OB1 dimerization led to shorter telomeres, which suggests that Cdc13 was deficient in recruitment of telomerase to the telomeres (Mitchell et al., 2010; Sun et al., 2011), whereas disruption of dimerization between the *Candida tropicalis* Cdc13 OB4 domains was shown to affect its ability to bind long telomeric DNA (Yu et al., 2012). Here, we demonstrate different consequences of disrupted dimerization between OB2 domains.

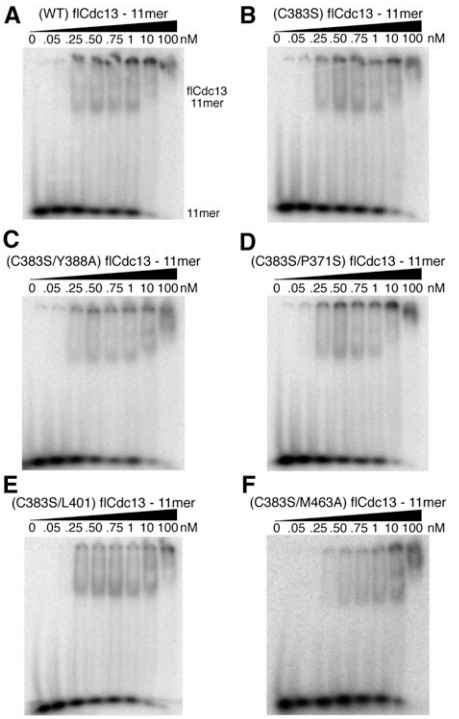

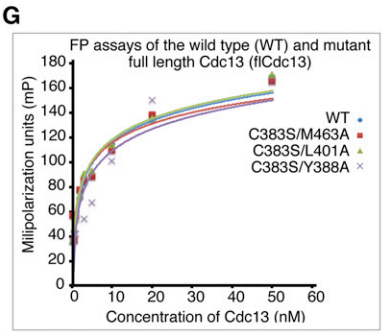

H

Cdc13 Construct	Protein	DNA Binding
Full length	Wild Type (WT)	+++
	Mutants	
	C383S	+++
	C383S/P371S	+++
	C383S/Y388A	+++
	C383S/L401A	+++
	C383S/M463A	+++
Truncation		
Res. 344-494	OB2 (WT)	ND*
*ND - Not Detected		

Figure 7. DNA Binding Properties of the WT and Mutant flCdc13 Proteins

(A–G) EMSA of (A) WT, flCdc13 – 11-mer, (B) C383S, flCdc13 – 11-mer, (C) C383S/P371S, flCdc13 –11-mer, (D) C383S/Y388A, flCdc13 – 11-mer, (E) C383S/L401A, flCdc13- 11-mer, (F) C383S/M463A, flCdc13 – 11-mer, and (G) fluorescence polarization (FP) assays of the full-length, WT, and mutant Cdc13 proteins using the yeast, telomeric DNA 12-mer (Table S1).

(H) Table of FP and EMSA values for the full-length, WT, and double-mutant Cdc13 proteins obtained from the curve fit of Figures 7A–7F.

Disruption of Cdc13 OB2 Dimerization Leads to Elongated Telomeres

Mutants designed to disrupt OB2 dimerization (C383S/P371S, C383S/Y388A, C383S/L401A, and C383S/M463A) lead to distinct phenotypes in vivo: (1) longer telomeres with decreased viability at elevated temperatures (C383S/P371S, C383S/Y388A, and C383S/L401A) (Figures 8A and 8B), which is in agreement with earlier studies of the Cdc13-1 protein that has only the P371S mutation (Garvik et al., 1995; Maringele and Lydall, 2002; Nugent et al., 1996; Zubko et al., 2004), and (2) longer telomeres without affecting cell viability at elevated temperatures (C383S/M463A) (Figures 8A and 8B).

The structure presented here provides a clear framework within which the phenotypes of the above mutants can be interpreted. P371 terminates β2 and is critical for the initiation and overall organization of coil 1 by forcing it into a specific direction, which is required for proper folding and productive homodimerization of OB2 (Figures 4C, 5A, and 5B). Mutating P371 to a serine would most likely alter the organization of coil 1, leading to disruption of multiple contacts between the two OB2 monomers and to some extent the fold of this domain explaining why this single-point mutant has such detrimental effects on Cdc13 function and cell viability. The fact that the *cdc13-1* (P371S) mutant is partially viable at room temperature can be explained by the crosslinking data, which shows that although OB2 dimerization is severely reduced (78%), it is not completely eliminated (Figures 3B and 3C). Similarly, mutation of the hydrophobic side chains of Y388 and L401 to alanine disrupts direct contacts with the hydrophobic side chain of the conserved M463, thus destabilizing the dimer interface, albeit to a lesser extent (70% and 50%, respectively) than the *cdc13-1* mutation (Figures 3B and 3C). The fact that Y388A and L401A are not viable at elevated temperatures could be explained by the fact that these residues, like P371S, are also involved in the fold of OB2. In particular, Y388A and L401A mediate contacts that are essential for the fold of coil 2 (Figure 5C), which is also required for the proper architecture of this domain. Clearly, disruption of the Y388 and L401 contacts could lead to the reorganization of coil 2, an effect enhanced at elevated temperatures, leading to a dysfunctional Cdc13 and cell death. The fact that Y388A and L401A mutants are not as temperature sensitive as *cdc13-1* could be explained by the reduced number of residue-residue contacts that are disrupted by these mutations within the same monomer when compared to those disrupted by the P371S mutation. Consistent with this hypothesis, the Y388A mutation shows reduced cellular viability at 30°C and is completely inviable at 37°C. As expected, the smaller hydrophobic side chain of the L401A mutant shows temperature sensitivity only at 37°C. This hypothesis is further supported by the fact that the M463A mutation, which is only involved in extensive OB2 dimer interactions and not the fold of the domain (Figure 4D), shows elongated telomeres but does not show any temperature-related growth defects. The ability of the above Cdc13 mutants to maintain cell viability at room temperature suggests that although the mutants disrupt binding between isolated Cdc13 and Stn1 in vitro, the proteins may still associate to some degree in vivo, a notion supported by our crosslinking data (Figures 3B and 3C). This may occur via the aid of mutual interacting partners, including Ten1 and telomeric ssDNA, which could stabilize to some extent, the Cdc13-Stn1 interaction in vivo.

Disruption of Cdc13 OB2 Dimerization Prevents Productive Cdc13-Stn1 Association

Elongated telomeres can be caused by a defective CST complex that is unable to (1) cap the ends of chromosomes and/or (2) bring Polα to the telomeres for C-strand synthesis. Stn1 is located at the core of these processes, where it is required for the proper assembly of the CST complex and is involved in the recruitment of Polα to the telomeres (Chandra et al., 2001; Gasparyan et al., 2009; Grossi et al., 2004; Puglisi et al., 2008). Biochemical data presented here show that the C383S/P371S,

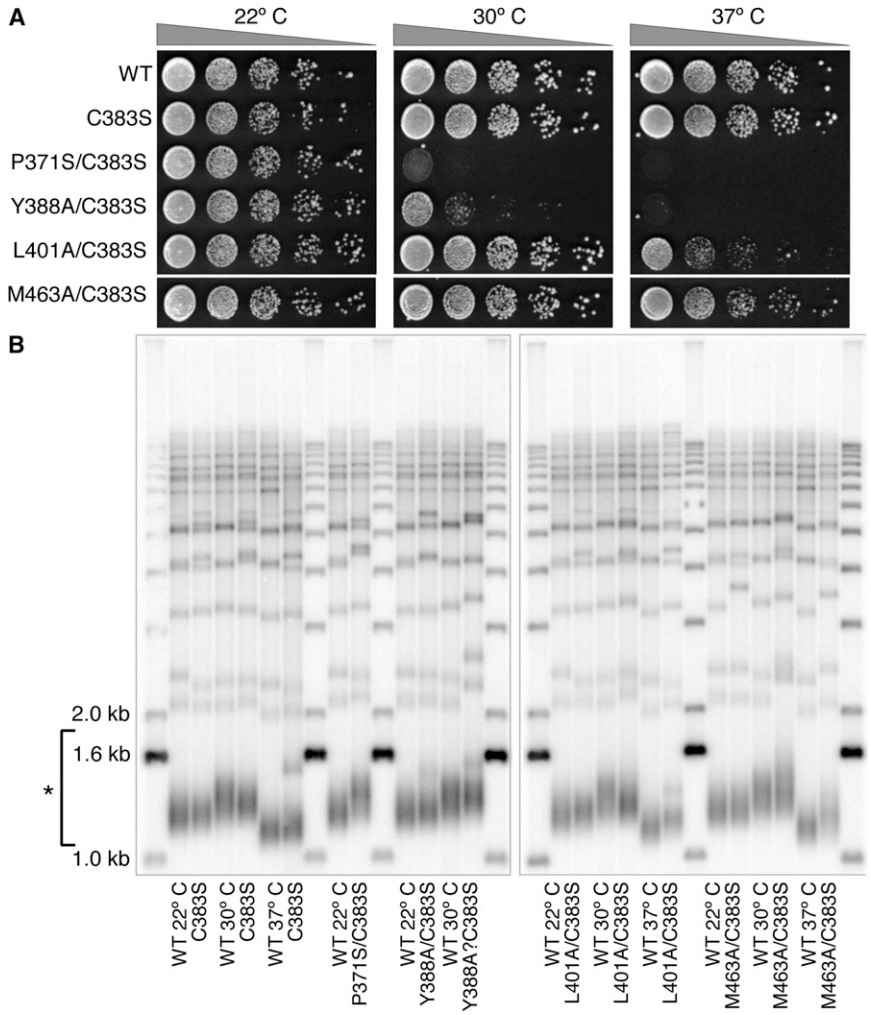

Figure 8. Spot Assays and Southern Blots of Cells with WT or Mutant flCdc13

(A) Cdc13 OB2 dimerization mutants display temperature-dependent defects in cell viability.

(B) Cdc13 OB2 dimerization mutants display temperature-dependent increases in telomere length by Southern blot analysis. Telomere blots show all mutations (if viable) at the indicated temperatures. The samples in each panel are flanked by a labeled ladder with molecular weights indicated at left. *The terminal Y' telomere fragments.

C383S/Y388A, C383S/L401A, and C383S/M463A mutations abolish Cdc13-Stn1 binding (Figures 6C–6E) even though our data suggests that there are not significant and direct contacts between OB2 and Stn1 (Figure S1A). However, there is extensive evidence showing that both the RD (located upstream of the OB2) (Bianchi et al., 2004; Chandra et al., 2001; Nugent et al., 1996; Tseng et al., 2006) and CTD (DeZwaan et al., 2009; Hang et al., 2011) of Cdc13 are implicated in Stn1 binding. For example, the Cdc13-2 (E252K) RD mutant is defective for Stn1 binding both in vitro (DeZwaan et al., 2009) and in vivo (Chandra et al., 2001; Nugent et al., 1996). Also, phosphorylation of the RD T308 residue acts as a switch that regulates Stn1 versus Est1 binding (Li et al., 2009), whereas sumoylation of the CTD of Cdc13 leads to increased Cdc13-Stn1 binding (Hang et al., 2011). The fact that Cdc13-Stn1 association is mediated by two distant locations of Cdc13 (RD and CTD)—a notion also supported by our ITC data (Figures 6D and S1C)—suggests distinct domain organization of Cdc13 to facilitate Stn1 contact with these domains. Taken together, the structural biochemical and functional data on Cdc13 and its interacting partners suggests that the Cdc13 dimer adopts a permanent or transient structure that brings the CTD and RD domains either in direct contact or in close proximity to each other forming a Stn1-interacting interface. The notion that the CTD is in close proximity with the N-terminal portion of Cdc13 is further supported by the fact that subunits of DNA polymerase α interact with both Stn1 (Grossi et al., 2004) and the N-terminal portion of Cdc13 (Sun et al., 2011). It is possible then that the local structural organization of the binding interface of Cdc13 for Stn1 is dependent on OB2 dimerization. Disruption of the OB2 dimer leads to RD restructuring and downregulation of Stn1 binding. Loss of proper Stn1 binding to Cdc13 leads to inefficient CST assembly, telomere uncapping, and loss of cell viability. Simultaneously, the RD becomes accessible for Est1 binding and telomerase recruitment to the telomeres, leading to telomere elongation (Figure 8). Moreover, loss of Stn1 binding to Cdc13 could affect Pol α recruitment to the telomeres, where it is involved in C-strand replication and has been implicated in telomere length maintenance (Grossi et al., 2004; Hsu et al., 2004; Qi and Zakian, 2000). The above model, based on a host of structural, biochemical, and functional assays, sheds some light into the complex mechanism of Cdc13 function. However, the structure of the full-length Cdc13 is required for a clear view of the complex domain organization and mechanistic understanding of this essential protein.

EXPERIMENTAL PROCEDURES

Protein Expression and Purification

The *S. cerevisiae* Cdc13 OB2, comprising residues 344 to 494, was identified via limited proteolysis and cloned into a pET28b vector with a cleavable hexahistidine tag (his-tag) at the N terminus. The protein was overexpressed in *Escherichia coli* BL21-CodonPlus(DE3)-RIPL cells (Stratagene, La Jolla, CA, USA) at 20°C for 4 hr, using 1 mM IPTG (isopropyl-β-D-thiogalactopyranoside; Gold Biotechnology, St. Louis, MO, USA). Cells were lysed in a buffer containing 25 mM Tris.HCl, 0.5 M KCl, 5 mM 2-mercaptoethanol, 5% glycerol, 1 mM phenylmethylsulfonyl fluoride (PMSF), and 1 mM benzamidine (pH 7.5) via sonication. The protein was purified using Ni-NTA (QIAGEN, Hilden, Germany), followed by TEV cleavage of the his-tag, HS-poros (PerSpectiveBiosystems [Applied Biosystems], Foster City, CA, USA) and size-exclusion chromatography using a Superdex S200 10/300 column (S200 - GE Healthcare). The

Table 1. Data Collection, Phasing, and Refinement Statistics

	Native 1	Hg Derivative
Data Collection		
Space group	$P2_12_12_1$	$P2_12_12_1$
Cell dimensions		
a, *b*, *c* (Å)	40.9, 78.8, 100.7	41.2, 79.2, 101.6
α, β, γ (°)		
Resolution (Å)	40–2.3 (2.42–2.3)[a]	50–2.85 (2.95–2.85)
R_{sym} or R_{merge}	8.4 (47.1)	13.9 (47.6)
$I/\sigma I$	14.4 (3.2)	10.5 (2.8)
Completeness (%)	99.28 (96.2)	100 (100)
Redundancy	6.7 (5.6)	6.6 (6.9)
Phasing Analysis		
Resolution (Å)		40–2.85
R_{cullis} (anom)		0.85
Number of sites		4
Mean figure of merit (FOM)		0.34
Refinement		
Resolution (Å)	40–2.3	
No. reflections	14,202	
R_{work}/ R_{free}	20.4/24.6	
No. atoms		
Protein	2,035	
Water	110	
B-factors		
Protein	30.97	
Water	39.6	
Rmsd		
Bond lengths (Å)	0.010	
Bond angles (°)	1.553	
Ramachandran plot (%)		
Most favored	90.7	
Allowed	9.3	

[a]Parentheses represent highest resolution shell.

WT and mutant, flCdc13 proteins were cloned into a modified pET28b vector expressing a TEV cleavable, N-terminal, his-tag followed by a sumo fusion protein. The proteins were overexpressed in *E. coli* BL21-CodonPlus(DE3)-RIPL cells (Stratagene) at 20°C overnight in 2YT media and 1 mM IPTG. The cells were harvested by centrifugation and resuspended in buffer containing 25 mM Tris.HCl, 0.5 M KCl, 5 mM 2-mercaptoethanol, 5% glycerol, 1 mM PMSF, and 1 mM benzamidine (pH 7.5). Cells were lysed by sonication and purified over a Ni.NTA (QIAGEN) column followed by ion exchange (HS poros - PerSpectiveBiosystems) and S200 chromatography.

Protein Crystallization and Data Collection

The pure Cdc13, OB2 protein (~25 mg/ml) was dialyzed in 5 mM Tris.HCl, 100 mM KCl, and 1 mM TCEP (pH 7.5) prior to crystallization trials. Using the Hampton Research crystallization screens, we obtained two crystal forms, one belonging to the orthorhombic $P2_12_12_1$ and the other to the tetragonal $P432_12$ space groups (Table 1). The orthorhombic crystals were prepared by mixing 1 volume of protein with 1 volume of 0.1 M NaCl, 0.1 M BIS-Tris (pH 6.5), and 1.5 M $AmSO_4$. Crystals were harvested in cryoprotectant containing crystallization solution and 30% glycerol. The tetragonal crystals were prepared by mixing the protein with 0.49 M NaH_2PO_4 monohydrate and 0.91 M Na_2HPO_4 at 1:1 ratio. Data were collected at the National Synchrotron Light Source (NSLS), beamlines X29 and X25 and were processed with HKL2000 (Otwinowski and Minor, 1997) or MOSFLM (Leslie, 1992), as implemented in ELVES (Holton and Alber, 2004). The orthorhombic crystals, which diffracted to higher resolution (2.3 Å) than the tetragonal ones (2.9 Å) were used in this study (Table 1).

Structure Determination and Refinement

Initial phases were obtained by the method of single anomalous dispersion (SAD) to 3.5 Å resolution using a methyl mercury chloride ($MeHgCl_2$) derivative (Table 1). The derivative was prepared by soaking the crystals with 5 mM $MeHgCl_2$ for 1 minute. Heavy atom sites were located and phases calculated using SOLVE (Brünger et al., 1998) and density modification was performed with RESOLVE (Terwilliger, 1999). The model was built in COOT (Emsley and Cowtan, 2004) using the cysteine positions determined from the mercury sites as guideposts to trace the protein sequence. The model was refined using REFMAC5 (Murshudov et al., 2011) and CNS SOLVE (Brünger et al., 1998). Figures were prepared in PyMOL (http://www.pymol.org).

Electrophoretic Mobility Shift Assays

The sstDNA was radiolabeled with γ-ATP (10 μCi/μl) using T4 polynucleotide kinase (New England Biolabs, Ipswich, MA, USA). The labeling reactions were incubated at 37°C for 1 hr and stopped with 10 mM EDTA and incubation at 95°C for 5 min. The reactions were spun down in a Microspin G-25 column (GE Healthcare) to remove excess nucleotides. The radiolabeled DNA probes were used at 1 nM for OB2 and 0.5 nM for flCdc13 with increasing protein concentrations (OB2 - 0, 0.1, 0.3, 0.4, 0.5, 0.6, 0.8, 1, 2, and 2.5 μM; flCdc13 – 0, 0.05, 0.1, 0.25, 0.5, 0.75, 1, 10, and 100 nM). The binding reactions were carried out in a buffer containing 20 mM Tris.HCl (pH 8.0), 75 mM $MgCl_2$, 1 mM EDTA, and 1 mM DTT. Reaction mixtures were incubated on ice for 45 min and subsequently run on a 6% DNA retardation gel (Invitrogen, Carlsbad, CA, USA) with 0.5x Tris-borate-EDTA (TBE) buffer on ice for 50 minutes at 100 V. Gels were dried, exposed overnight on a storage phosphor screen (GE Healthcare), and analyzed using ImageQuant software (Molecular Dynamics, Sunnyvale, CA, USA).

Formaldehyde Crosslinking

Crosslinking experiments were carried out as described in Nadeau and Carlson (2007c). The Cdc13 OB2 and flCdc13, WT and mutant proteins were diluted to 0.5 and 0.15 mg/ml, respectively, in a buffer containing 20 mM HEPES (pH 7.5), 100 mM KCl, 1 mM TCEP, and 2.5% glycerol. Crosslinking was performed by mixing 4 μl of 1.5% formaldehyde (final concentration 0.3%) to 20 μl of protein and incubating at room temperature for 90 min. The crosslinking reaction was stopped by adding 5 μl of 1.5 M Tris.HCl (pH 8.0) to the reaction mix. The products of the crosslinking experiment were then run on a 15% SDS-PAGE gel, and the band intensities were analyzed with ImageJ (Abramoff et al., 2004).

Dynamic Light Scattering

Dynamic light scattering experiments were carried out using the DynaPro Titan (Wyatt Technology). Cdc13 OB2 protein samples were tested in various buffer conditions in which the salt, glycerol concentration, and temperature varied. The buffer conditions tested are as follows: Buffer A – 25 mM Tris.HCl, 5% glycerol, 0.5 M KCl, and 1 mM TCEP (pH 7.5); Buffer B – 5 mM Tris.HCl, 250 mM KCl, and 1 mM Tris.HCl (pH 7.5); Buffer C – 5 mM Tris.HCl, 100 mM KCl, and 1 TCEP (pH 7.5). All four samples were placed in a 12 μl, 8.5 mm Center Height quartz cell and tested at 4°C and 25°C. All protein samples showed a single peak corresponding to 100% mass at around 2.78 nM corresponding to a 38 KDa protein, which corresponds to the size of the dimeric OB2.

Isothermal Titration Calorimetry

ITC experiments were carried out at 20°C and 30°C, and all protein samples were prepared in a buffer containing 25 mM HEPES (pH 7.5), 175 mM KCl, 5% v/v glycerol, and 1 mM TCEP. The experiments were performed by titrating the C-terminal domain of Stn1, residues 311–494 (Stn1C) (stock concentration, 610 μM) into a measuring cell containing WT or mutant flCdc13

at 40 μM and 60 μM, respectively, using a MicroCal ITC200 and VPITC (GE Healthcare). The data was analyzed with Origin 7 (Microcal).

Fluorescence Polarization

We performed FP DNA binding reactions in 10 μl samples using a Wallac EnVision Plate reader (PerkinElmer, Waltham, MA, USA). The binding reactions were carried out in a buffer containing 20 mM Tris.HCl (pH 8.0), 75 mM $MgCl_2$, 1 mM EDTA, and 1 mM DTT. The 12-mer and 43-mer DNA probes were purchased with a 5′, 6-carboxyfluorescein tag (6-FAM from IDT). The final probe concentration used was 5 nM, whereas the OB2 and flCdc13 protein concentrations ranged from 0 to 2 μM and 0 to 50 nM, respectively. The reactions were incubated at room temperature for 5 minutes and pipetted in triplicate into a black 384-well ProxiPlate (PerkinElmer). The reactions were excited with 490 nm light, and the emissions were measured at 520 nm. The milipolarization values were calculated by the Envision operating software (PerkinElmer), and the binding constants were determined using Prism5 (GraphPad Software).

Yeast Strains and Plasmids

Functional experiments were performed in the BY4743 background of *S. cerevisiae*. The various Cdc13 OB2 serine and alanine point mutations were introduced into a pRS415-based plasmid (a derivative of pVL1091 lacking the *EST1* open reading frame, a gift of V. Lundblad) expressing *CDC13* under the control of its own promoter, as previously described (Mitchell et al., 2010). *CDC13*/*cdc13Δ*:*kanMX* diploid cells (YBJ641) transformed with the WT or mutant *CDC13* plasmids were sporulated and haploid *cdc13Δ* cells containing the pRS415 plasmid of interest were obtained by tetrad dissection. The cells were grown in synthetic complete medium lacking Leu (SC–Leu), as a selection system for the plasmid (Amberg et al., 2005).

Cell Viability Assays

Haploid cells containing the pRS415 plasmid with Cdc13 OB2 mutations were grown in SC-Leu at 22°C overnight in a roller drum until they reached log phase growth. Cell counts were taken with a Coulter Counter, and the cultures were diluted in sterile water to 10^5 cells/15 μl. The cells were serially diluted to 10^4, 10^3, 10^2, and 10 cells/15 μl. A volume of approximately 15 μl of each dilution was stamped onto Sc-Leu plates with a frogger. The plates were incubated at 22°C, 30°C, and 37°C for 2–3 days. All spots are from the same plate.

Telomere Southern Blots

We performed Southern blots on DNA harvested from cultures grown to approximately 90 generations in SC-Leu at three different temperatures, 22°C, 30°C, and 37°C, and samples were prepared essentially as described in Mitchell et al. (2010). XhoI-digested DNA was separated in a 1% agarose gel and transferred under denaturing alkaline conditions to a Hybond-XL membrane. The probe was derived from a cloned 330 base pair *S. cerevisiae* telomere repeat fragment (an MluI to BamHI fragment purified from pBJ1313), which was random hexamer labeled with α-^{32}P dCTP. We concurrently labeled a 1 KB+ DNA ladder sample. Blots were hybridized with both probes at 65°C overnight in Church's buffer, washed with 2X SCC/1% SDS, 0.3X SSC/0.2% SDS, and 0.2X SSC/0.1% SDS at 65°C and then imaged with a phosphorimager.

ACCESSION NUMBERS

The coordinates and structure factors of the Cdc13 OB2 protein has been deposited in the Research Collaboratory for Structural Bioinformatics (RCSB) databank under the accession number 3HCE.

SUPPLEMENTAL INFORMATION

Supplemental Information includes one table and two figures and can be found with this article online at http://dx.doi.org/10.1016/j.str.2012.10.012.

ACKNOWLEDGMENTS

Thanks to the Lieberman lab for use of the ITC instrumentation. This project was funded by the Pennsylvania Department of Health, the V Foundation, the Emerald Foundation, the National Institutes of Health, and the National Institute on Aging. E.S. and M.M. designed the research and analyzed the data; M.M. performed the research; D.S. assisted with the FP assays; F.B.J. and J.J.W. performed the in vivo studies; and E.S. and M.M. wrote the paper with contributions from F.B.J. and J.J.W.

Received: July 30, 2012
Revised: September 29, 2012
Accepted: October 20, 2012
Published online: November 21, 2012

REFERENCES

Abramoff, M.D., Magalhaes, P.J., and Ram, S.J. (2004). Image processing with ImageJ. Biophotonics International *11*, 36–42.

Amberg, D.C., Burke, D.J., and Strathern, J.N. (2005). Methods in Yeast Genetics 2005 (Cold Spring Harbor, NY: Cold Spring Harbor Press).

Baumann, P., Podell, E., and Cech, T.R. (2002). Human Pot1 (protection of telomeres) protein: cytolocalization, gene structure, and alternative splicing. Mol. Cell. Biol. *22*, 8079–8087.

Bianchi, A., Negrini, S., and Shore, D. (2004). Delivery of yeast telomerase to a DNA break depends on the recruitment functions of Cdc13 and Est1. Mol. Cell *16*, 139–146.

Blackburn, E.H., and Gall, J.G. (1978). A tandemly repeated sequence at the termini of the extrachromosomal ribosomal RNA genes in Tetrahymena. J. Mol. Biol. *120*, 33–53.

Brünger, A.T., Adams, P.D., Clore, G.M., DeLano, W.L., Gros, P., Grosse-Kunstleve, R.W., Jiang, J.S., Kuszewski, J., Nilges, M., Pannu, N.S., et al. (1998). Crystallography & NMR system: A new software suite for macromolecular structure determination. Acta Crystallogr. D Biol. Crystallogr. *54*, 905–921.

Chandra, A., Hughes, T.R., Nugent, C.I., and Lundblad, V. (2001). Cdc13 both positively and negatively regulates telomere replication. Genes Dev. *15*, 404–414.

DeZwaan, D.C., Toogun, O.A., Echtenkamp, F.J., and Freeman, B.C. (2009). The Hsp82 molecular chaperone promotes a switch between unextendable and extendable telomere states. Nat. Struct. Mol. Biol. *16*, 711–716.

Emsley, P., and Cowtan, K. (2004). Coot: model-building tools for molecular graphics. Acta Crystallogr. D Biol. Crystallogr. *60*, 2126–2132.

Gao, H., Cervantes, R.B., Mandell, E.K., Otero, J.H., and Lundblad, V. (2007). RPA-like proteins mediate yeast telomere function. Nat. Struct. Mol. Biol. *14*, 208–214.

Garvik, B., Carson, M., and Hartwell, L. (1995). Single-stranded DNA arising at telomeres in cdc13 mutants may constitute a specific signal for the RAD9 checkpoint. Mol. Cell. Biol. *15*, 6128–6138.

Gasparyan, H.J., Xu, L., Petreaca, R.C., Rex, A.E., Small, V.Y., Bhogal, N.S., Julius, J.A., Warsi, T.H., Bachant, J., Aparicio, O.M., and Nugent, C.I. (2009). Yeast telomere capping protein Stn1 overrides DNA replication control through the S phase checkpoint. Proc. Natl. Acad. Sci. USA *106*, 2206–2211.

Gelinas, A.D., Paschini, M., Reyes, F.E., Héroux, A., Batey, R.T., Lundblad, V., and Wuttke, D.S. (2009). Telomere capping proteins are structurally related to RPA with an additional telomere-specific domain. Proc. Natl. Acad. Sci. USA *106*, 19298–19303.

Grandin, N., Reed, S.I., and Charbonneau, M. (1997). Stn1, a new Saccharomyces cerevisiae protein, is implicated in telomere size regulation in association with Cdc13. Genes Dev. *11*, 512–527.

Grandin, N., Damon, C., and Charbonneau, M. (2001). Cdc13 prevents telomere uncapping and Rad50-dependent homologous recombination. EMBO J. *20*, 6127–6139.

Grossi, S., Puglisi, A., Dmitriev, P.V., Lopes, M., and Shore, D. (2004). Pol12, the B subunit of DNA polymerase alpha, functions in both telomere capping and length regulation. Genes Dev. *18*, 992–1006.

Gustafsson, C., Rhodin Edsö, J., and Cohn, M. (2011). Rap1 binds single-stranded DNA at telomeric double- and single-stranded junctions and competes with Cdc13 protein. J. Biol. Chem. *286*, 45174–45185.

Hang, L.E., Liu, X., Cheung, I., Yang, Y., and Zhao, X. (2011). SUMOylation regulates telomere length homeostasis by targeting Cdc13. Nat. Struct. Mol. Biol. *18*, 920–926.

Holton, J., and Alber, T. (2004). Automated protein crystal structure determination using ELVES. Proc. Natl. Acad. Sci. USA *101*, 1537–1542.

Horvath, M.P., Schweiker, V.L., Bevilacqua, J.M., Ruggles, J.A., and Schultz, S.C. (1998). Crystal structure of the Oxytricha nova telomere end binding protein complexed with single strand DNA. Cell *95*, 963–974.

Hsu, C.L., Chen, Y.S., Tsai, S.Y., Tu, P.J., Wang, M.J., and Lin, J.J. (2004). Interaction of Saccharomyces Cdc13p with Pol1p, Imp4p, Sir4p and Zds2p is involved in telomere replication, telomere maintenance and cell growth control. Nucleic Acids Res. *32*, 511–521.

Hughes, T.R., Weilbaecher, R.G., Walterscheid, M., and Lundblad, V. (2000). Identification of the single-strand telomeric DNA binding domain of the Saccharomyces cerevisiae Cdc13 protein. Proc. Natl. Acad. Sci. USA *97*, 6457–6462.

Kaushansky, A., Allen, J.E., Gordus, A., Stiffler, M.A., Karp, E.S., Chang, B.H., and MacBeath, G. (2010). Quantifying protein-protein interactions in high throughput using protein domain microarrays. Nat. Protoc. *5*, 773–790.

Lei, M., Podell, E.R., Baumann, P., and Cech, T.R. (2003). DNA self-recognition in the structure of Pot1 bound to telomeric single-stranded DNA. Nature *426*, 198–203.

Lei, M., Podell, E.R., and Cech, T.R. (2004). Structure of human POT1 bound to telomeric single-stranded DNA provides a model for chromosome end-protection. Nat. Struct. Mol. Biol. *11*, 1223–1229.

Leslie, A.G.W. (1992). Recent changes to the MOSFLM package for processing film and image plate data. Joint CCP4 ESF-EAMCB Newsl. Protein Crystallogr. *26*.

Li, S., Makovets, S., Matsuguchi, T., Blethrow, J.D., Shokat, K.M., and Blackburn, E.H. (2009). Cdk1-dependent phosphorylation of Cdc13 coordinates telomere elongation during cell-cycle progression. Cell *136*, 50–61.

Lin, J.J., and Zakian, V.A. (1996). The Saccharomyces CDC13 protein is a single-strand TG1-3 telomeric DNA-binding protein in vitro that affects telomere behavior in vivo. Proc. Natl. Acad. Sci. USA *93*, 13760–13765.

Maringele, L., and Lydall, D. (2002). EXO1-dependent single-stranded DNA at telomeres activates subsets of DNA damage and spindle checkpoint pathways in budding yeast yku70Delta mutants. Genes Dev. *16*, 1919–1933.

Martín, V., Du, L.L., Rozenzhak, S., and Russell, P. (2007). Protection of telomeres by a conserved Stn1-Ten1 complex. Proc. Natl. Acad. Sci. USA *104*, 14038–14043.

Mitchell, M.T., Smith, J.S., Mason, M., Harper, S., Speicher, D.W., Johnson, F.B., and Skordalakes, E. (2010). Cdc13 N-terminal dimerization, DNA binding, and telomere length regulation. Mol. Cell. Biol. *30*, 5325–5334.

Mitton-Fry, R.M., Anderson, E.M., Hughes, T.R., Lundblad, V., and Wuttke, D.S. (2002). Conserved structure for single-stranded telomeric DNA recognition. Science *296*, 145–147.

Mitton-Fry, R.M., Anderson, E.M., Theobald, D.L., Glustrom, L.W., and Wuttke, D.S. (2004). Structural basis for telomeric single-stranded DNA recognition by yeast Cdc13. J. Mol. Biol. *338*, 241–255.

Miyake, Y., Nakamura, M., Nabetani, A., Shimamura, S., Tamura, M., Yonehara, S., Saito, M., and Ishikawa, F. (2009). RPA-like mammalian Ctc1-Stn1-Ten1 complex binds to single-stranded DNA and protects telomeres independently of the Pot1 pathway. Mol. Cell *36*, 193–206.

Murshudov, G.N., Skubák, P., Lebedev, A.A., Pannu, N.S., Steiner, R.A., Nicholls, R.A., Winn, M.D., Long, F., and Vagin, A.A. (2011). REFMAC5 for the refinement of macromolecular crystal structures. Acta Crystallogr. D Biol. Crystallogr. *67*, 355–367.

Nadeau, O.W., and Carlson, G.M. (2007a). Protein interactions captured by chemical cross-linking: One-step cross-linking with formaldehyde. CSH Protoc. *2007*, pdb prot4634.

Nadeau, O.W., and Carlson, G.M. (2007b). Protein interactions captured by chemical cross-linking: Simple cross-linking screen using Sulfo-MBS. CSH Protoc. *2007*, pdb prot4587.

Nadeau, O.W., and Carlson, G.M. (2007c). Protein interactions captured by chemical cross-linking: Two-step cross-linking with ANB*NOS. CSH Protoc. *2007*, pdb prot4635.

Nakaoka, H., Nishiyama, A., Saito, M., and Ishikawa, F. (2012). Xenopus laevis Ctc1-Stn1-Ten1 (xCST) protein complex is involved in priming DNA synthesis on single-stranded DNA template in Xenopus egg extract. J. Biol. Chem. *287*, 619–627.

Nandakumar, J., Podell, E.R., and Cech, T.R. (2010). How telomeric protein POT1 avoids RNA to achieve specificity for single-stranded DNA. Proc. Natl. Acad. Sci. USA *107*, 651–656.

Nugent, C.I., Hughes, T.R., Lue, N.F., and Lundblad, V. (1996). Cdc13p: a single-strand telomeric DNA-binding protein with a dual role in yeast telomere maintenance. Science *274*, 249–252.

Otwinowski, Z., and Minor, W. (1997). Processing of X-ray diffraction data collected in oscillation mode. In Methods in Enzymology, C.W. Carter and R.M. Sweets, eds. (Charlottesville: University of Virginia), pp. 307–326.

Paschini, M., Toro, T.B., Lubin, J.W., Braunstein-Ballew, B., Morris, D.K., and Lundblad, V. (2012). A naturally thermolabile activity compromises genetic analysis of telomere function in Saccharomyces cerevisiae. Genetics *191*, 79–93.

Pennock, E., Buckley, K., and Lundblad, V. (2001). Cdc13 delivers separate complexes to the telomere for end protection and replication. Cell *104*, 387–396.

Prescott, J., and Blackburn, E.H. (1997). Functionally interacting telomerase RNAs in the yeast telomerase complex. Genes Dev. *11*, 2790–2800.

Puglisi, A., Bianchi, A., Lemmens, L., Damay, P., and Shore, D. (2008). Distinct roles for yeast Stn1 in telomere capping and telomerase inhibition. EMBO J. *27*, 2328–2339.

Qi, H., and Zakian, V.A. (2000). The Saccharomyces telomere-binding protein Cdc13p interacts with both the catalytic subunit of DNA polymerase alpha and the telomerase-associated est1 protein. Genes Dev. *14*, 1777–1788.

Sharma, K., Weber, C., Bairlein, M., Greff, Z., Kéri, G., Cox, J., Olsen, J.V., and Daub, H. (2009). Proteomics strategy for quantitative protein interaction profiling in cell extracts. Nat. Methods *6*, 741–744.

Song, X., Leehy, K., Warrington, R.T., Lamb, J.C., Surovtseva, Y.V., and Shippen, D.E. (2008). STN1 protects chromosome ends in Arabidopsis thaliana. Proc. Natl. Acad. Sci. USA *105*, 19815–19820.

Sun, J., Yu, E.Y., Yang, Y., Confer, L.A., Sun, S.H., Wan, K., Lue, N.F., and Lei, M. (2009). Stn1-Ten1 is an Rpa2-Rpa3-like complex at telomeres. Genes Dev. *23*, 2900–2914.

Sun, J., Yang, Y., Wan, K., Mao, N., Yu, T.Y., Lin, Y.C., DeZwaan, D.C., Freeman, B.C., Lin, J.J., Lue, N.F., and Lei, M. (2011). Structural bases of dimerization of yeast telomere protein Cdc13 and its interaction with the catalytic subunit of DNA polymerase α. Cell Res. *21*, 258–274.

Surovtseva, Y.V., Churikov, D., Boltz, K.A., Song, X., Lamb, J.C., Warrington, R., Leehy, K., Heacock, M., Price, C.M., and Shippen, D.E. (2009). Conserved telomere maintenance component 1 interacts with STN1 and maintains chromosome ends in higher eukaryotes. Mol. Cell *36*, 207–218.

Terwilliger, T.C. (1999). Reciprocal-space solvent flattening. Acta Crystallogr. D Biol. Crystallogr. *55*, 1863–1871.

Tseng, S.F., Lin, J.J., and Teng, S.C. (2006). The telomerase-recruitment domain of the telomere binding protein Cdc13 is regulated by Mec1p/Tel1p-dependent phosphorylation. Nucleic Acids Res. *34*, 6327–6336.

Wang, F., Podell, E.R., Zaug, A.J., Yang, Y., Baciu, P., Cech, T.R., and Lei, M. (2007). The POT1-TPP1 telomere complex is a telomerase processivity factor. Nature *445*, 506–510.

Wang, M.J., Lin, Y.C., Pang, T.L., Lee, J.M., Chou, C.C., and Lin, J.J. (2000). Telomere-binding and Stn1p-interacting activities are required for the

essential function of Saccharomyces cerevisiae Cdc13p. Nucleic Acids Res. *28*, 4733–4741.

Wellinger, R.J. (2009). The CST complex and telomere maintenance: the exception becomes the rule. Mol. Cell *36*, 168–169.

Xu, L., Petreaca, R.C., Gasparyan, H.J., Vu, S., and Nugent, C.I. (2009). TEN1 is essential for CDC13-mediated telomere capping. Genetics *183*, 793–810.

Yu, E.Y., Sun, J., Lei, M., and Lue, N.F. (2012). Analyses of Candida Cdc13 orthologues revealed a novel OB fold dimer arrangement, dimerization-assisted DNA binding, and substantial structural differences between Cdc13 and RPA70. Mol. Cell. Biol. *32*, 186–198.

Zubko, M.K., Guillard, S., and Lydall, D. (2004). Exo1 and Rad24 differentially regulate generation of ssDNA at telomeres of Saccharomyces cerevisiae cdc13-1 mutants. Genetics *168*, 103–115.

